Unit Commitment with an Enhanced Natural Gas-Flow Model

Sheng Chen, *Student Member, IEEE,* Antonio J. Conejo, *Fellow, IEEE,* Ramteen Sioshansi, *Senior Member, IEEE,* and Zhinong Wei

***Abstract*—The interdependency of electric power and natural gas systems requires co-ordinated operational planning. We propose a unit commitment model that integrates a second-order-cone relaxation of a non-convex nonlinear natural gas flow model that considers pipeline line-pack. The model is enhanced by using convex envelopes of bilinear terms, which tighten the relaxation. By fixing the binary variables at their optimal values and linearizing the natural gas-flow-balance equations around the solution that is obtained, we obtain electricity and natural gas locational marginal prices as the dual variables of electricity- and natural gas-flow-balance equations, respectively. The interdependence between these sets of prices is discussed. Numerical results from two test systems validate the solution-quality and computational-efficiency benefits of the proposed modeling methodology.**

***Index Terms*—Power system operations, natural gas, unit commitment, second-order cone programming**

NOMENCLATURE

Indices, Sets, and Functions

$\mathbb{C}(m)$	set of natural gas compressors connected to node m
$E(i)$	set of power system buses directly connected to bus i
E_B	set of transmission lines
$E_v(i)$	set of generating units connected to bus i
$G(m)$	set of natural gas nodes connected to node m
G_B	set of natural gas pipelines
$G_P(m)$	set of natural gas-fired generating units connected to node m
$G_w(m)$	set of natural gas suppliers connected to node m
i, j	indices of power system buses in set, Ω_E
k	index of natural gas compressors in set, G_C
m, n	indices of natural gas-system nodes in set, Ψ_G
REF	reference bus of the power system
t	index of time periods in set, T
v	index of generating units in set, Ω
w	index of natural gas suppliers in set, Ψ_S
Ω_G	set of natural gas-fired generating units
Ω_R	set of coal-fired generating units

This work was supported by National Natural Science Foundation of China grant 51877071 and National Science Foundation grants 1548015 and 1808169.

S. Chen and Z. Wei are with the College of Energy and Electrical Engineering, Hohai University, Nanjing 210098, China (e-mail: chenshenghhu@163.com; wzn_nj@263.net).

A. J. Conejo is with the Department of Integrated Systems Engineering and the Department of Electrical and Computer Engineering, The Ohio State University, Columbus, OH 43210, USA (e-mail: conejonavarro.1@osu.edu).

R. Sioshansi is with the Department of Integrated Systems Engineering, The Ohio State University, Columbus, OH 43210, USA (e-mail: sioshansi.1@osu.edu).

Parameters and Constants

C_{EL}	value of lost electric load [\$/p.u.]
C_{GL}	value of lost natural gas load [\$/Mm^3]
$C_{G,v}$	variable production cost of coal-fired unit v [\$/p.u.]
$C_{O,v}$	non-fuel variable operation and maintenance cost of natural gas-fired unit v [\$/p.u.]
$C_{S,w}$	variable production cost of natural gas supplier w [\$/Mm^3]
$C_{\text{SD},v}$	shutdown cost of generating unit v [\$/shutdown]
$C_{\text{SU},v}$	start-up cost of generating unit v [\$/start-up]
$F_{L,m,t}$	non-generation-related natural gas demand at node m in time period t [Mm^3/h]
$F^{\max}_{C,k}$	natural gas-transportation limit of compressor k [Mm^3/h]
$F^{\max}_{S,w}$	maximum natural gas supply of supplier w [Mm^3/h]
$F^{\min}_{S,w}$	minimum natural gas supply of supplier w [Mm^3/h]
$F^{\text{ramp}}_{S,w}$	ramping limit of natural gas supplier w [Mm^3/h/(time period)]
$K_{m,n}$	line-pack parameter of pipeline connecting nodes m and n [(Mm^3)/bar]
$L_{\min}$	minimum total line-pack in natural gas system [Mm^3]
$P_{L,i,t}$	electric demand at bus i in time period t [p.u.]
$P^{\max}_{G,v}$	maximum output of generating unit v [p.u.]
$P^{\min}_{G,v}$	minimum output of generating unit v when it is online [p.u.]
$P^{\max}_{i,j}$	capacity of transmission line connecting buses i and j [p.u.]
$P^{\text{ramp}}_{G,v}$	ramping limit of generating unit v [p.u./(time period)]
$W_{m,n}$	Weymouth constant of pipeline connecting nodes m and n [(Mm^3/h)/bar]
Δ	duration of time periods [h]
η_v	heat rate of natural gas-fired unit v [Mm^3/h/p.u.]
ϑ_k	conversion efficiency of natural gas compressor k
$\pi^{\max}_m$	maximum natural gas pressure at node m [bar]
$\pi^{\min}_m$	minimum natural gas pressure at node m [bar]
$\rho^{\max}_k$	maximum compression ratio of natural gas compressor k
$\rho^{\min}_k$	minimum compression ratio of natural gas compressor k
$\sigma_{i,j}$	susceptance of transmission line connecting buses i and j [p.u.]

Variables

$F_{C,k,t}$	natural gas flow in time period t through compressor k [Mm^3/h]

$F^D_{L,m,t}$ non-generation-related natural gas demand at node m that is served in time period t [Mm^3/h]
$F_{G,v,t}$ fuel consumed by natural gas-fired generating unit v in time period t [Mm^3/h]
$F_{m,n,t}$ natural gas flow in time period t through pipeline connecting nodes m and n [Mm^3/h]
$\bar{F}_{m,n,t}$ average natural gas flow in time period t through pipeline connecting nodes m and n [Mm^3/h]
$F_{S,w,t}$ natural gas supplied in time period t by supplier w [Mm^3/h]
$L_{m,n,t}$ line-pack in time period t in pipeline connecting nodes m and n [Mm^3]
$P^D_{L,i,t}$ electric demand at bus i that is served in time period t [p.u.]
$P_{G,v,t}$ active power produced in time period t by generating unit v [p.u.]
$u_{G,v,t}$ binary variable that equals 1 if generating unit v is online in time period t and equals 0 otherwise
$y_{G,v,t}$ binary variable that equals 1 if generating unit v is started up in time period t and equals 0 otherwise
$z_{G,v,t}$ binary variable that equals 1 if generating unit v is shutdown in time period t and equals 0 otherwise
$\theta_{i,t}$ phase angle of bus i in time period t [rad]
$\pi^{\text{in}}_{k,t}$ inlet pressure of natural gas compressor k in time period t [bar]
$\pi_{m,t}$ natural gas pressure at node m in time period t [bar]
$\pi^{\text{out}}_{k,t}$ outlet pressure of natural gas compressor k in time period t [bar]
$\tau_{k,t}$ natural gas consumed by natural gas compressor k in time period t [Mm^3/h]

I. Introduction

ELECTRIC power and natural gas systems are becoming increasingly interdependent [1], [2]. This is driven by the low cost of natural gas-fired generating units. Moreover, many natural gas-fired units can provide the operating flexibility that high penetrations of renewable energy require [3]–[5]. Despite the growing interdependencies between these systems, they are typically planned and operated independently of one another. This lack of co-ordination can give rise to suboptimal operating decisions and can even raise security, reliability, or resilience issues. For instance, the United States experienced a large-scale electricity- and natural gas-service disruption in February, 2011, which highlights the challenges that this interdependency creates [6].

Given this context, co-ordinating the operation of the two systems is becoming increasingly important. The technical literature provides a number of approaches to such co-ordination. Liu *et al*. [7] propose a security-constrained unit commitment model that incorporates natural gas-pipeline constraints. The model is solved using Benders' decomposition, wherein the natural gas flows are represented using linear subproblems. Liu *et al*. [8] incorporate a transient natural gas-flow model, using a bilevel modeling approach. Their work takes the operation of the power system to be the upper-level problem, and includes natural gas-flow feasibility in the lower level. Zhao *et al*. [9] develop a two-stage stochastic unit commitment problem that includes natural gas-supply and -price uncertainties. Zhang *et al*. [10] propose a stochastic unit commitment model that considers transmission and generator outages and demand response. Correa-Posada *et al*. [11] consider transmission and pipeline contingencies within an integrated unit commitment model. He *et al*. [12] propose a two-stage robust unit commitment model that accounts for the natural gas system in making power system-operation decisions. Antenucci and Sansavini [13] investigate the impacts of natural gas-system constraints on a stochastic unit commitment model with $(N-1)$ contingency constraints.

A major challenge that these works contend with is that natural gas flows are highly nonlinear and non-convex. Some works [9]–[11] ignore these complexities (*i.e*., model linear natural gas flows or approximate them as being piecewise linear) while others [7], [8], [13] use nonlinear optimization models, which raise tractability issues. Another approach is to convexify the flow equations. Doing so allows some of the nonlinearities to be captured, while mitigating the challenges that non-convexity raises. Sanchez *et al*. [14] propose using a second-order-cone (SOC) relaxation to represent natural gas flows for expansion planning of natural gas and electric power systems. Other works [12] employ SOC relaxations for modeling optimal power and natural gas flows in co-ordinated operational-planning. Chen *et al*. [15] develop both steady-state and transient natural gas-flow models that employ SOC relaxations. The objective functions of their models are tailored to ensure tight solutions. Chen *et al*. [16] propose an enhanced SOC relaxation of a natural gas-flow model for dispatching electric power and natural gas systems. Wang *et al*. [17] propose a market-clearing model for natural gas that uses an SOC relaxation of the network.

SOC relaxations of natural gas-flow models represent a tradeoff between fidelity and computational tractability. The methods in the existing literature that employ SOC relaxations do leave some important gaps. Many methods [12], [14], [15] employ steady-state natural gas-flow models that neglect line-pack in pipelines. However, it is normally important to consider line-pack for short-term operational planning [18]. Moreover, many of the models in the existing literature that employ SOC relaxations yield solutions with relatively large feasibility gaps. These infeasibilities are often exacerbated if line-pack is considered. This implies that the models may be unsuitable for operating a system without heuristic refinement of a solution to find meaningful operating decisions.

Our work seeks to fill this gap in the literature on SOC relaxations of natural gas flows. Specifically, we propose a unit commitment model that has embedded within it non-convex and nonlinear natural gas-flow equations that represent line-pack. This unit commitment problem is a mixed-integer nonlinear optimization problem. We then employ an enhanced SOC relaxation that provides tighter feasibility bounds compared to natural gas-flow models in the existing literature that employ SOC relaxations. The enhanced SOC relaxation is based on convex envelopes of bilinear terms in the nonlinear natural gas-flow equations. An iterative bound-tightening algorithm is used to tighten the relaxation. With this relaxation, our unit commitment problem becomes a mixed-integer second-order cone problem (MISOCP). Using a small four-node ex-

ample and a large case study that is based on the IEEE 118-bus test system, we demonstrate the performance of our enhanced MISOCP compared to the standard SOC relaxation that is in the literature, demonstrating its tighter feasibility gaps. We also investigate the interdependencies between electric and natural gas locational marginal prices (LMPs) by examining the impacts of congestion in one system on LMPs in both systems.

The remainder of this paper is organized as follows. Section II presents the mixed-integer nonlinear unit commitment model with integrated natural gas-flow equations. Section III details the enhanced SOC relaxation, which yields the MISOCP. Sections IV and V summarize the results of the example and case study, respectively. Section VI concludes.

II. Model Formulation

We present here the formulation of our 'base' model (*i.e.*, the mixed-integer nonlinear optimization problem without any relaxation of the natural gas-flow constraints). This model includes a linearized dc representation of power flows and non-convex and nonlinear natural gas-flow constraints that capture line-pack [19]. The natural gas-flow constraints that we model are derived from a temporal and spatial discretization (using finite differences) of the partial differential equations that characterize pipeline dynamics and we use dimensional equations in the natural gas system [19], [20]. The power flows could be represented using a nonlinear ac model. Doing so would raise further tractability issues, in addition to those that arise from representing natural gas flows. Linearized dc models are normally used for day-ahead power system operation, which is the envisioned use of our proposed model. Moreover, our focus is on modeling natural gas flows, to which the representation of power flows is not germane.

The model is formulated as:

$$\min \sum_{t\in T}\Bigg[\sum_{v\in\Omega}\left(C_{\text{SU},v}y_{G,v,t}+C_{\text{SD},v}z_{G,v,t}\right) + \sum_{v\in\Omega_R}C_{G,v}P_{G,v,t}+\sum_{v\in\Omega_G}C_{O,v}P_{G,v,t} + \sum_{w\in\Psi_S}C_{S,w}F_{S,w,t}+\sum_{i\in\Omega_E}C_{\text{EL}}\cdot\left(P_{L,i,t}-P^D_{L,i,t}\right) + \sum_{m\in\Psi_G}C_{\text{GL}}\cdot\left(F_{L,m,t}-F^D_{L,m,t}\right)\Bigg] \tag{1}$$

$$\text{s.t.} \sum_{v\in E_v(i)}P_{G,v,t}-P^D_{L,i,t}=\sum_{j\in E(i)}\sigma_{i,j}\cdot(\theta_{i,t}-\theta_{j,t});\ \forall i\in\Omega_E,t\in T \tag{2}$$

$$P^{\min}_{G,v}u_{G,v,t}\le P_{G,v,t}\le P^{\max}_{G,v}u_{G,v,t};\forall v\in\Omega,t\in T \tag{3}$$

$$-P^{\text{ramp}}_{G,v}\le P_{G,v,t}-P_{G,v,t-1}\le P^{\text{ramp}}_{G,v};\ \forall v\in\Omega,t\in T \tag{4}$$

$$y_{G,v,t}-z_{G,v,t}=u_{G,v,t}-u_{G,v,t-1};\forall v\in\Omega,t\in T \tag{5}$$

$$u_{G,v,t},y_{G,v,t},z_{G,v,t}\in\{0,1\};\forall v\in\Omega,t\in T \tag{6}$$

$$-P^{\max}_{i,j}\le\sigma_{i,j}\cdot(\theta_{i,t}-\theta_{j,t})\le P^{\max}_{i,j};\ \forall(i,j)\in E_B,t\in T \tag{7}$$

$$\theta_{\text{REF},t}=0;\forall t\in T \tag{8}$$

$$0\le P^D_{L,i,t}\le P_{L,i,t};\forall i\in\Omega_E,t\in T \tag{9}$$

$$\sum_{w\in G_w(m)}F_{S,w,t}-F^D_{L,m,t}-\sum_{k\in\mathbb{C}(m)}\tau_{k,t} - \sum_{v\in G_P(m)}F_{G,v,t}=\sum_{n\in G(m)}F_{m,n,t}+\sum_{k\in\mathbb{C}(m)}F_{C,k,t}\ \forall m\in\Psi_G,t\in T \tag{10}$$

$$\bar{F}_{m,n,t}=\frac{1}{2}(F_{m,n,t}-F_{n,m,t});\ \forall(m,n)\in G_B,t\in T \tag{11}$$

$$\bar{F}^2_{m,n,t}/W^2_{m,n}=\pi^2_{m,t}-\pi^2_{n,t};\forall(m,n)\in G_B,t\in T \tag{12}$$

$$L_{m,n,t}=\frac{1}{2}K_{m,n}\cdot(\pi_{m,t}+\pi_{n,t});\ \forall(m,n)\in G_B,t\in T \tag{13}$$

$$\Delta\cdot(F_{m,n,t}+F_{n,m,t})=L_{m,n,t}-L_{m,n,t-1};\ \forall(m,n)\in G_B,t\in T \tag{14}$$

$$\tau_{k,t}=\vartheta_kF_{C,k,t};\forall k\in G_C,t\in T \tag{15}$$

$$\rho^{\min}_k\pi^{\text{in}}_{k,t}\le\pi^{\text{out}}_{k,t}\le\rho^{\max}_k\pi^{\text{it}}_{k,t};\forall k\in G_C,t\in T \tag{16}$$

$$0\le F_{C,k,t}\le F^{\max}_{C,k,t};\forall k\in G_C,t\in T \tag{17}$$

$$F^{\min}_{S,w}\le F_{S,w,t}\le F^{\max}_{S,w};\forall w\in\Psi_S,t\in T \tag{18}$$

$$-F^{\text{ramp}}_{S,w}\le F_{S,w,t}-F_{S,w,t-1}\le F^{\text{ramp}}_{S,w};\ \forall w\in\Psi_S,t\in T \tag{19}$$

$$\pi^{\min}_m\le\pi_{m,t}\le\pi^{\max}_m;\forall m\in\Psi_G,t\in T \tag{20}$$

$$\sum_{(m,n)\in G_B}L_{m,n,|T|}\ge L_{\min} \tag{21}$$

$$0\le F^D_{L,m,t}\le F_{L,m,t};\forall m\in\Psi_G,t\in T \tag{22}$$

$$F_{G,v,t}=\eta_vP_{G,v,t};\forall v\in\Omega_G,t\in T. \tag{23}$$

Objective function (1) gives the total cost of operating the power and natural gas systems. The first two terms represent the start-up and shutdown costs, respectively, of generating units. The third term represents the variable cost of coal-fired units while the fourth term represents the non-fuel variable cost of natural gas-fired units. The fifth term represents natural gas-production costs. This term implicitly includes the cost of supplying fuel to natural gas-fired units. The final remaining terms represent the costs of curtailing electric and natural gas demands, respectively.

The model has three sets of constraints. The first set, constraints (2)–(9), pertain to the operation of the electric power system. Constraints (2) impose load balance at each bus. Constraints (3) and (4) impose capacity and ramping limits, respectively, on the generating units. Constraints (5) define the start-up and shutdown variables for the generating units in terms of changes in the corresponding 'online' state variables while constraints (6) enforce integrality of these variables. Constraints (7) define power flows along each transmission line in terms of differences in the phase angles at its ends and constraints (8) set the phase angle at the reference bus equal to zero. Constraints (9) limit the load that is served at each bus by demand.

The second set of constraints, (10)–(22), pertain to the natural gas system. Constraints (10) impose nodal flow balance. Constraints (11) define the average flow in each pipeline

in terms of flows in each direction. Constraints (12) relate these average natural gas flows to the change in squared pressure between the two ends of each pipeline. We assume that $F_{m,n,t} \geq 0$, meaning that we know the direction of the flows *a priori*. This is a reasonable assumption in day-ahead operations [21], whereas longer-term planning exercises should consider bi-directional natural gas flows. Constraints (13) determine the line-pack on pipelines based on the upstream and downstream pressures at their ends. Constraints (14) give the relationship between hourly changes in flows and line-pack in pipelines. Constraints (15) compute the fuel consumption of natural gas-driven compressors in the network. Constraints (16) impose minimum and maximum compressor ratios while constraints (17) impose flow limits. Constraints (18) and (19) impose capacity and ramping limits, respectively, on natural gas suppliers. Constraints (20) limit the nodal pressures. Constraint (21) imposes a minimum line-pack level in the final time period of the optimization horizon, thereby ensuring that the natural gas in the network is not depleted. Constraints (22) limit load served at each node by nodal demand.

The final set of constraints, (23), couple the two systems through the fuel consumption of natural gas-fired units.

III. Enhanced SOC-Based Relaxation of Natural Gas-Flow Model

Integrated model (1)–(23) is a mixed-integer nonlinear optimization problem that has a non-convex continuous relaxation. Specifically, tractability issues arise from constraint set (12), which can be equivalently written as:

$$\bar{F}^2_{m,n,t}/W^2_{m,n} \leq \pi^2_{m,t} - \pi^2_{n,t}; \forall (m,n) \in G_B, t \in T \quad (24)$$

$$\bar{F}^2_{m,n,t}/W^2_{m,n} \geq \pi^2_{m,t} - \pi^2_{n,t}; \forall (m,n) \in G_B, t \in T. \quad (25)$$

A standard technique to convexify such a model is to relax (25), thereby replacing (12) with the SOC constraints (24) [14], [22]. Doing so yields a MISOCP, which can be solved using off-the-shelf software tools. However, the solutions that are obtained from such a relaxation may yield non-trivial violations of constraint set (12).

Building off of this approach, we propose employing an enhanced SOC relaxation that includes a convex relaxation of (25). To convexify (25) we replace the bilinear terms that appear in the inequalities with their convex envelopes [23], [24]. To do so, we define two sets of variables, $a_{m,n,t}$ and $b_{m,n,t}$, which are defined as the sums and differences of the pressure at the two ends of each pipeline *via* the equalities:

$$a_{m,n,t} = \pi_{m,t} + \pi_{n,t}; \forall (m,n) \in G_B, t \in T \quad (26)$$

$$b_{m,n,t} = \pi_{m,t} - \pi_{n,t}; \forall (m,n) \in G_B, t \in T. \quad (27)$$

We also define two new sets of auxiliary variables, $\kappa_{m,n,t}$ and $\lambda_{m,n,t}$. The convex relaxation of (25) is given by:

$$\kappa_{m,n,t}/W^2_{m,n} \geq \lambda_{m,n,t}; \forall (m,n) \in G_B, t \in T \quad (28)$$

$$\kappa_{m,n,t} \geq \bar{F}^2_{m,n,t}; \forall (m,n) \in G_B, t \in T \quad (29)$$

$$\kappa_{m,n,t} \leq (F^{\max}_{m,n,t} + F^{\min}_{m,n,t})\bar{F}_{m,n,t} - F^{\max}_{m,n,t}F^{\min}_{m,n,t}; \forall (m,n) \in G_B, t \in T \quad (30)$$

$$\lambda_{m,n,t} \geq a^{\min}_{m,n,t}b_{m,n,t} + b^{\min}_{m,n,t}a_{m,n,t} - a^{\min}_{m,n,t}b^{\min}_{m,n,t}; \forall (m,n) \in G_B, t \in T \quad (31)$$

$$\lambda_{m,n,t} \geq a^{\max}_{m,n,t}b_{m,n,t} + b^{\max}_{m,n,t}a_{m,n,t} - a^{\max}_{m,n,t}b^{\max}_{m,n,t}; \forall (m,n) \in G_B, t \in T \quad (32)$$

$$\lambda_{m,n,t} \leq a^{\min}_{m,n,t}b_{m,n,t} + b^{\max}_{m,n,t}a_{m,n,t} - a^{\min}_{m,n,t}b^{\max}_{m,n,t}; \forall (m,n) \in G_B, t \in T \quad (33)$$

$$\lambda_{m,n,t} \leq a^{\max}_{m,n,t}b_{m,n,t} + b^{\min}_{m,n,t}a_{m,n,t} - a^{\max}_{m,n,t}b^{\min}_{m,n,t}; \forall (m,n) \in G_B, t \in T; \quad (34)$$

and (26), (27), where $F^{\min}_{m,n,t}$, $F^{\max}_{m,n,t}$, $a^{\min}_{m,n,t}$, $a^{\max}_{m,n,t}$, $b^{\min}_{m,n,t}$ and $b^{\max}_{m,n,t}$ are constants.

In this relaxation, $\kappa_{m,n,t}$ and $\lambda_{m,n,t}$ represent the convexified approximations of $\bar{F}^2_{m,n,t}$ and $\pi^2_{m,t} - \pi^2_{n,t}$, respectively. Thus, (28) 'replaces' (25), insomuch as it imposes the necessary relationship between $\kappa_{m,n,t}$ and $\lambda_{m,n,t}$. Fig. 1 shows the convexified bounds on the value of $\bar{F}^2_{m,n,t}$ that (29) and (30) impose on $\kappa_{m,n,t}$.

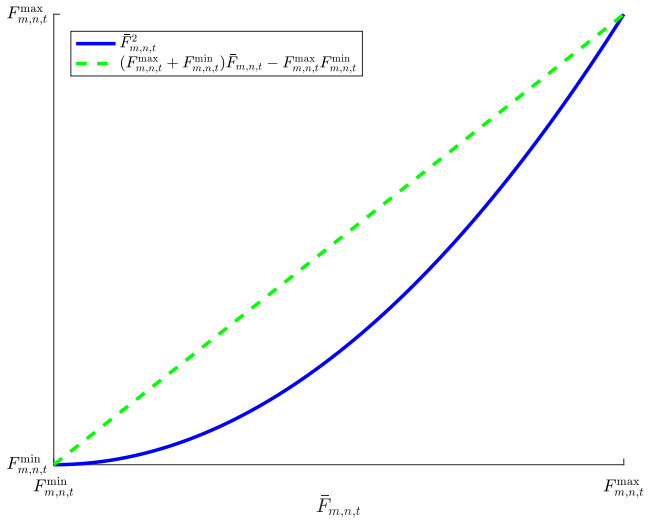

Fig. 1. Convexified approximation of $\bar{F}^2_{m,n,t}$ that is given by (29) and (30).

Constraints (31)–(34) impose analogous bounds on $\lambda_{m,n,t}$. To see this, first note that from the definition of $a_{m,n,t}$ and $b_{m,n,t}$, we have that $a_{m,n,t}b_{m,n,t} = \pi^2_{m,t} - \pi^2_{n,t}$. Constraints (31)–(34) impose bounds on $\lambda_{m,n,t}$ that are related to $a_{m,n,t}$ and $b_{m,n,t}$. Visualizing these bounds is challenging, because $a_{m,n,t}b_{m,n,t}$ is a surface and (31)–(34) are hyperplanes in a three-dimensional space. Fig. 2 shows $a_{m,n,t}b_{m,n,t}$ and (31)–(34) for the special case in which $a_{m,n,t} = b_{m,n,t}$. The figure shows that (31)–(34) provides a tight convex envelope that contains $a_{m,n,t}b_{m,n,t}$.

Thus, our proposed enhanced MISOCP, which we hereafter refer to as an eMISOCP, is given by (1)–(11), (13)–(23), (24), and (26)–(34). Relaxation (29)–(34) is not the only way to convexify (12). For instance, one can apply a convex envelope to each of the $\pi^2_{m,t}$ and $\pi^2_{n,t}$ terms that are on the right-hand side of (12) separately. However, convexifying each set of quadratic terms individually requires two sets of convex approximations, which typically results in a relatively less tight relaxation that may also entail added computational complexities.

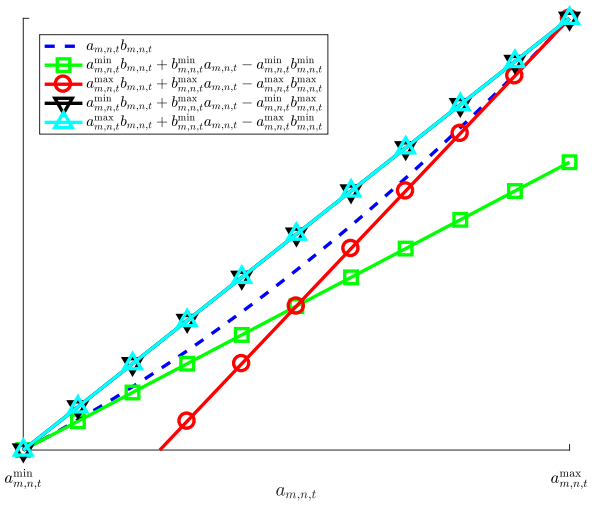

Fig. 2. Convexified approximation of $\pi^2_{m,t}-\pi^2_{n,t}$ that is given by (31)–(34).

Algorithm 1 eMISOCP bound-tightening

1: **input:** δ, sequence $\{\epsilon^k\}_{k=1}^K$
2: **initialize:** $k \leftarrow 1$; initialize values for $F^{\min}_{m,n,t}$, $F^{\max}_{m,n,t}$, $a^{\min}_{m,n,t}$, $a^{\max}_{m,n,t}$, $b^{\min}_{m,n,t}$, $b^{\max}_{m,n,t}$ $\forall (m,n) \in G_B, t \in T$
3: **repeat**
4: Solve eMISOCP to obtain $F^{\text{inc}}_{m,n,t}$, $a^{\text{inc}}_{m,n,t}$, $b^{\text{inc}}_{m,n,t}$ $\forall (m,n) \in G_B, t \in T$
5: $F^{\min}_{m,n,t} \leftarrow (1-\epsilon^k)F^{\text{inc}}_{m,n,t}, \forall (m,n) \in G_B, t \in T$
6: $F^{\max}_{m,n,t} \leftarrow (1+\epsilon^k)F^{\text{inc}}_{m,n,t}, \forall (m,n) \in G_B, t \in T$
7: $a^{\min}_{m,n,t} \leftarrow (1-\epsilon^k)a^{\text{inc}}_{m,n,t}, \forall (m,n) \in G_B, t \in T$
8: $a^{\max}_{m,n,t} \leftarrow (1+\epsilon^k)a^{\text{inc}}_{m,n,t}, \forall (m,n) \in G_B, t \in T$
9: $b^{\min}_{m,n,t} \leftarrow (1-\epsilon^k)b^{\text{inc}}_{m,n,t}, \forall (m,n) \in G_B, t \in T$
10: $b^{\max}_{m,n,t} \leftarrow (1+\epsilon^k)b^{\text{inc}}_{m,n,t}, \forall (m,n) \in G_B, t \in T$
11: $k \leftarrow k+1$
12: **until** $|\pi^2_{m,t}-\pi^2_{n,t}-\bar{F}^2_{m,n,t}/W^2_{m,n}|/\pi^2_{m,t} \leq \delta$ $\forall (m,n) \in G_B, t \in T$ **or** $k > K+1$

A. Tightening of Enhanced SOC Relaxation

Figs. 1 and 2 show that the tightness of the proposed convex envelopes that are given by (29)–(34) depend on the chosen values of $F^{\min}_{m,n,t}$, $F^{\max}_{m,n,t}$, $a^{\min}_{m,n,t}$, $a^{\max}_{m,n,t}$, $b^{\min}_{m,n,t}$ and $b^{\max}_{m,n,t}$. For example, the maximum error in approximating $\bar{F}^2_{m,n,t}$ is $[(F^{\max}_{m,n,t}-F^{\min}_{m,n,t})/2]^2$. This is because (29)–(34) allow $\kappa_{m,n,t}$ and $\lambda_{m,n,t}$ to lie anywhere within the convex envelopes that are given by the constraint sets. The farther the true values of $\bar{F}^2_{m,n,t}$ and $\pi^2_{m,t}-\pi^2_{n,t}$ are from $F^{\min}_{m,n,t}$ and $F^{\max}_{m,n,t}$ and $a^{\min}_{m,n,t}$, $a^{\max}_{m,n,t}$, $b^{\min}_{m,n,t}$ and $b^{\max}_{m,n,t}$, respectively, the less accurate the resulting relaxation is.

As such, we employ a simple bound-tightening algorithm to improve the proposed relaxation. Algorithm 1 provides pseudocode outlining the steps of this procedure. The algorithm takes two inputs on line 1. δ is a convergence tolerance and $\{\epsilon^k\}_{k=1}^K$ is a decreasing sequence of control parameters that is used to successively tighten the bounds on the convex envelopes. Line 2 initializes the algorithm by setting the iteration counter to 1 and starting with relatively wide bounds on the convex envelopes by choosing wide starting ranges for $F^{\min}_{m,n,t}$, $F^{\max}_{m,n,t}$, $a^{\min}_{m,n,t}$, $a^{\max}_{m,n,t}$, $b^{\min}_{m,n,t}$, and $b^{\max}_{m,n,t}$.

Lines 3–12 are the main iterative loop. The eMISOCP is solved using the current values of $F^{\min}_{m,n,t}$, $F^{\max}_{m,n,t}$, $a^{\min}_{m,n,t}$, $a^{\max}_{m,n,t}$, $b^{\min}_{m,n,t}$, and $b^{\max}_{m,n,t}$ in line 4. Solving the eMISOCP gives incumbent values for the convex relaxation, which we denote as $F^{\text{inc}}_{m,n,t}$, $a^{\text{inc}}_{m,n,t}$, and $b^{\text{inc}}_{m,n,t}$. Lines 5–10 then update the values of $F^{\min}_{m,n,t}$, $F^{\max}_{m,n,t}$, $a^{\min}_{m,n,t}$, $a^{\max}_{m,n,t}$, $b^{\min}_{m,n,t}$, and $b^{\max}_{m,n,t}$ using the incumbent values. The sequence, $\{\epsilon^k\}_{k=1}^K$, should decrease sufficiently slowly to ensure that the values of $F^{\min}_{m,n,t}$, $F^{\max}_{m,n,t}$, $a^{\min}_{m,n,t}$, $a^{\max}_{m,n,t}$, $b^{\min}_{m,n,t}$, and $b^{\max}_{m,n,t}$ converge to tightened envelopes without 'cutting off' an optimal solution. The algorithm continues for at most K iterations or until constraint set (12) is satisfied within the tolerance, δ.

B. Comparison of Natural Gas-Flow Models

We compare the performance of three models, using our example and case study. The first model, which we hereafter refer to as the MINLP, is given by (1)–(23). The MINLP is a nonlinear mixed-integer optimization problem with a non-convex continuous relaxation. Thus, we can only guarantee finding local optima. However, solutions that are obtained from the MINLP are guaranteed to strictly satisfy all of the constraints, including constraint set (12). The second model, which we hereafter refer to as the MISOCP, is given by (1)–(11), (13)–(23), and (24). The third model is the eMISOCP, in which the convex envelopes are updated using Algorithm 1.

We measure the performance of these models in terms of computation time and solution quality. Solution quality is measured in three ways. The first is the objective-function gap, which is defined as the percentage difference in the optimal objective-function value between the MINLP and each of the MISOCP and the eMISOCP. The objective-function gap measures how accurately each of the two relaxations represents the true cost of operating the power and natural gas systems.

Our second solution-quality metric is the violation of pipeline-flow constraint set (12). To compute this metric, we first define:

$$V_{m,n,t} = \frac{\pi^2_{m,t}-\pi^2_{n,t}-\bar{F}^2_{m,n,t}/W^2_{m,n}}{\pi^2_{m,t}}, \tag{35}$$

as the p.u. amount by which each of the MISOCP and eMISOCP solutions violate constraint (12) in time step t for the pipeline connecting nodes m and n. We then compute:

$$V_{\text{S}} = 100 \times \frac{\sum_{t\in T;(m,n)\in G_B} V_{m,n,t}}{|T|\cdot|G_B|}, \tag{36}$$

as the average (over time steps and pipelines) percentage violation of constraint set (12) for each of the MISOCP and eMISOCP solutions.

Our third-solution quality metric is related to the violation of pipeline-flow constraint set (12). For this third metric we first fix a slack natural gas-supply node, which should be a node with a relatively high supply capacity. We then fix all of the variables pertaining to the operation of the electric power system (*i.e.*, all of the values of $F_{G,v,t}$, $P^D_{L,i,t}$, $P_{G,v,t}$, $u_{G,v,t}$, $y_{G,v,t}$, $z_{G,v,t}$, and $\theta_{i,t}$), the natural gas injections (*i.e.*, the $F_{S,w,t}$'s) for all of the nodes except for the slack node, and

the natural gas pressures (*i.e.*, the $\pi_{m,t}$'s) for the slack node *only* to the final values that are obtained from each of the MISOCP and eMISOCP solutions. Constraints (10)–(15) are then solved using Newton's method to obtain a solution that is feasible in all of the equality constraints that pertain to the natural gas system [5]. The value of (1) that corresponds to these solutions that are obtained from Newton's method measures the actual cost of operating the natural gas system following the solutions given by the MISOCP and eMISOCP.

C. Electric and Natural Gas LMPs

Electric and natural gas LMPs can be obtained from problem (1)–(23) by fixing the binary variables to their optimal values and solving the resulting continuous relaxation. The dual variables that are associated with constraint set (2) are standard electric LMPs, which are differentiated by time period and bus. Analogously, the dual variables that are associated with constraint set (10) give natural gas LMPs, which are differentiated by time and node. One challenge that can arise from using this latter set of dual variables is that the SOC relaxations can introduce numerical instabilities [25]. This issue can be overcome by linearizing the three sets of quadratic terms in constraint set (12) around the final solution. This linearization is given by:

$$[(\bar{F}^*_{m,n,t})^2 + 2\bar{F}^*_{m,n,t} \cdot (\bar{F}_{m,n,t} - \bar{F}^*_{m,n,t})]/W^2_{m,n} = (\pi^*_{m,t})^2 + 2\pi^*_{m,t} \cdot (\pi_{m,t} - \pi^*_{m,t}) - (\pi^*_{n,t})^2 - 2\pi^*_{n,t} \cdot (\pi_{n,t} - \pi^*_{n,t}); \forall (m,n) \in G_B, t \in T; \quad (37)$$

where $\bar{F}^*_{m,n,t}$, $\pi^*_{m,t}$, and $\pi^*_{n,t}$ denote the optimized values of these variables. Constraint set (37) can be substituted for constraint set (12), the binary variables fixed to their optimal values, and the resulting continuous relaxation can be solved to obtain stable electric and natural gas LMPs.

IV. Example

This section summarizes the results of a four-bus/four-node example, the topology of which is shown in Fig. 3. Buses, nodes, loads, natural gas supplies, and generators are labeled using the same notation as in the model formulation. Natural gas-fired unit 2 couples the two systems. All of the pertinent data are provided in an online supplement.[1] We examine system operations in a base case as well as two additional cases in which non-generation-related natural gas demands are increased by 10% and 20% relative to the baseline.

Table I summarizes the objective-function values of the three models and the corresponding objective-function gaps. In all of the cases (with baseline and increased natural gas demands), the eMISOCP outperforms the MISOCP by providing a more accurate estimate of the true cost of operating the two systems. Fig. 4 shows, as a demonstrative example, the values of $V_{1,3,t}$, as defined by (35), in each of the hours with natural gas demands that are 20% above baseline. As expected, the eMISOCP results in significantly reduced constraint violations compared to the MISOCP, which has violations in all hours. Table II summarizes the values of V_S

[1]https://doi.org/10.6084/m9.figshare.6025340.v1

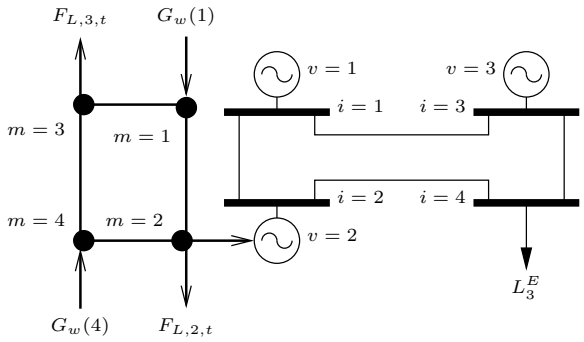

Fig. 3. System topology of the example in Section IV.

that are obtained from the eMISOCP across six iterations of Algorithm 1. For comparison, the MISOCP yields a solution with a value of $V_S = 43.7\%$. These results show that the eMISOCP outperforms the MISOCP in terms of average constraint violations. Moreover, Table II shows that Algorithm 1 obtains progressively better solutions with smaller constraint violations as the value of ϵ is reduced.

TABLE I
Objective Function Values [$ Million] and Gaps [%] For Example In Section IV

	Base Line		10% Higher		20% Higher	
Model	Value	Gap	Value	Gap	Value	Gap
MINLP	3.296	–	3.595	–	3.943	–
MISOCP	3.286	0.3	3.582	0.4	3.907	0.9
eMISOCP	3.296	0.0	3.593	0.1	3.933	0.3

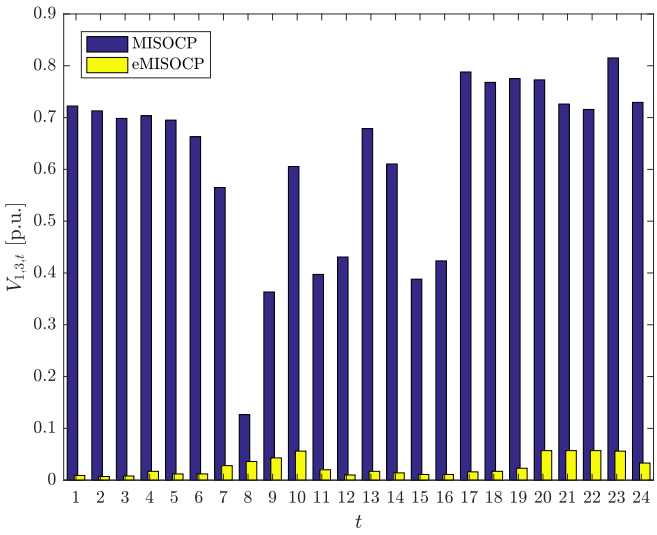

Fig. 4. Violations of constraints (12) for natural gas pipeline connecting nodes 1 and 3 in the example in Section IV.

The final solutions that are given by the MISOCP and eMISOCP slightly violate the node-2 minimum natural gas-pressure constraint in hour 12. The natural gas pressures that are given by the MISOCP and eMISOCP solutions are 29.4 bar and 29.9 bar, whereas the minimum pressure in 30 bar. If Newton's method is employed to obtain a feasible solution

TABLE II
AVERAGE VIOLATION OF CONSTRAINT SET (12) IN SOLUTIONS OBTAINED FROM SIX ITERATIONS OF ALGORITHM 1 IN THE EXAMPLE IN SECTION IV

Iteration Number	ϵ	V_S [%]
1	–	13.4
2	0.50	5.3
3	0.25	2.5
4	0.20	1.9
5	0.15	1.5
6	0.10	1.2

from the MISOCP and eMISOCP, the resulting operating cost, as measured by (1), is \$3.299 million and \$3.297 million, respectively. This illustrates a further benefit of the proposed eMISOCP, insomuch as feasibly operating the system using the solution that is obtained from this model is less costly than using the MISOCP solution.

Figs. 5 and 6 illustrate the interdependencies between natural gas and electric LMPs and how the cost of operating the two systems are interrelated. Fig. 5 shows hourly load-weighted natural gas LMPs that are obtained from the eMISOCP. All three of the cases result in high LMPs in hours 9–12, which is more pronounced in the cases with higher natural gas demands. The higher LMPs in the high-demand cases are due to congestion in the natural gas system, which results in unavoidable curtailment of natural gas demand. This curtailment increases the operating cost of natural gas-fired unit 2 during these hours, yielding the increased electric LMPs that are shown in Fig. 6.

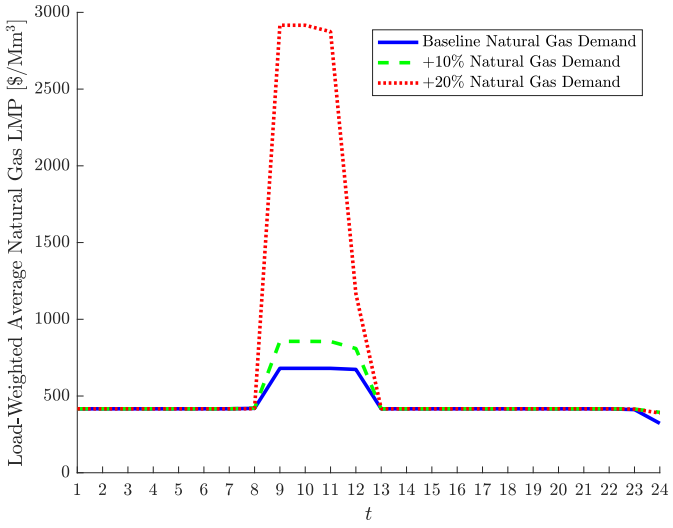

Fig. 5. Load-weighted average natural gas LMPs obtained from applying eMISOCP to the example in Section IV.

The high natural gas LMPs in hours 9–12 have a further spillover effect, in that they reduce the use of natural gas-fired generation. The case with baseline natural gas demands yields about 19 GWh of natural gas-fired generation during the day that is modeled. This is reduced to 17 GWh and 13 GWh in the cases in which natural gas demands are 10% and 20% above baseline, respectively. As such, natural gas-system congestion

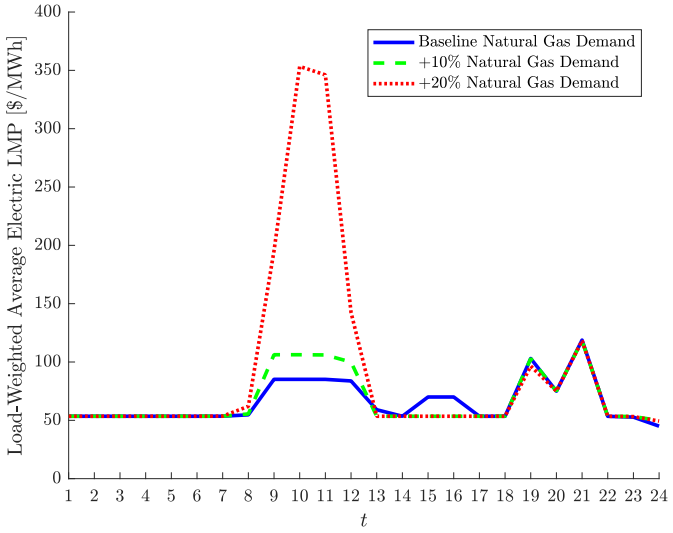

Fig. 6. Load-weighted average electric LMPs obtained from applying eMISOCP to the example in Section IV.

restricts the use of natural gas-fired generation and increases electric LMPs.

The three models are implemented in version 24.7 of the GAMS mathematical modeling software package. The MINLP is solved using DICOPT and the MISOCP and eMISOCP are solved using CPLEX with default solver settings. All of the models are solved on a computer with a 1.9 GHz Intel Core processor and 4 GB of memory. The MINLP, MISOCP, and eMISOCP require approximately 6.1 s, 1.3 s, and 7.3 s, respectively, of wall-clock time to solve.

V. CASE STUDY

This section summarizes the results of a case study, which consists of the IEEE 118-bus system, which is coupled with the 48-node natural gas system that is shown in Fig. 7. Nodes, natural gas supplies and loads, and power system nodes that have natural gas-fired units (which couple the systems) are labeled using the same notation that is used in the model formulation. Natural gas compressors are represented by the trapezoids. Natural gas-system data are obtained from the work of Wu *et al.* [26]. The nine natural gas-fired units constitute 36% of the total generating capacity in the power system.

Tables III and IV and Fig. 8 summarize the relative performance of the MISOCP and eMISOCP in terms of objective-function value and constraint violations. Table III shows that the eMISOCP yields a more accurate estimate of the cost of the operating the two systems. Fig. 8 shows, as a representative example, the constraint violations for all of the natural gas pipelines in hour 15. The MISOCP yields a solution with a value of $V_S = 16.6\%$. Comparing this to the values that are reported in Table IV further illustrates the performance of the eMISOCP in reducing constraint violations. Overall, these results show that the improved performance of the eMISOCP carries over to this larger case study.

To further explore interactions between the two systems, we consider three cases with different amounts of transmission capacity available in the electric power system. Specifically,

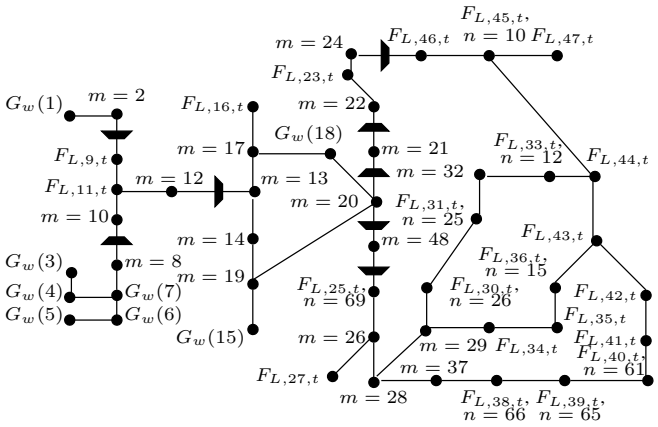

Fig. 7. Natural gas-system topology of the case study in Section V.

TABLE III
OBJECTIVE FUNCTION VALUES [$ MILLION] AND GAPS [%] FOR CASE STUDY IN SECTION V

Model	Value	Gap
MINLP	44.29	–
MISOCP	43.81	1.1
eMISOCP	44.21	0.2

we consider a base case, which corresponds to the IEEE 118-bus system and two additional cases in which all branches are assumed to have transmission capacities that are 20% and 40% below the baseline.

Fig. 9 shows day-ahead load-weighted electricity LMPs in the three cases when the eMISOCP is used. The third case, with 40% less transmission capacity relative to the baseline, has the highest overall prices, due to extreme transmission congestion. Fig. 10 shows the amount of natural gas-fired generation in the three cases. Because natural gas is a relatively expensive generation fuel (compared to coal), natural gas-fired generators are only used in the case study when lower-cost alternatives cannot be. Fig. 10 shows that transmission congestion exacerbates the need to use natural gas-fired generation, leading to the higher electric LMPs that are shown in Fig. 9. The increased reliance on natural gas-fired units in the two cases with lower transmission capacity leads to higher natural gas LMPs, as shown in Fig. 11. Thus, the natural gas and electric LMPs tend to increase together.

The case study is implemented using the same computational environment with which the example is. The MINLP, MISOCP, and eMISOCP each require approximately 375 minutes, 41 minutes, and 105 minutes of wall-clock time, respectively, to find a solution. Contrasting these computation times with the example in Section IV shows that the MISOCP and eMISOCP scale better than the MINLP does. Moreover, use of the eMISOCP introduces a tradeoff. While it provides higher-quality solutions than the MISOCP, this entails an added computational cost.

TABLE IV
AVERAGE VIOLATION OF CONSTRAINT SET (12) IN SOLUTIONS OBTAINED FROM THREE ITERATIONS OF ALGORITHM 1 IN THE CASE STUDY IN SECTION V

Iteration Number	ϵ	V_S [%]
1	–	2.4
2	0.50	2.0
3	0.25	0.8

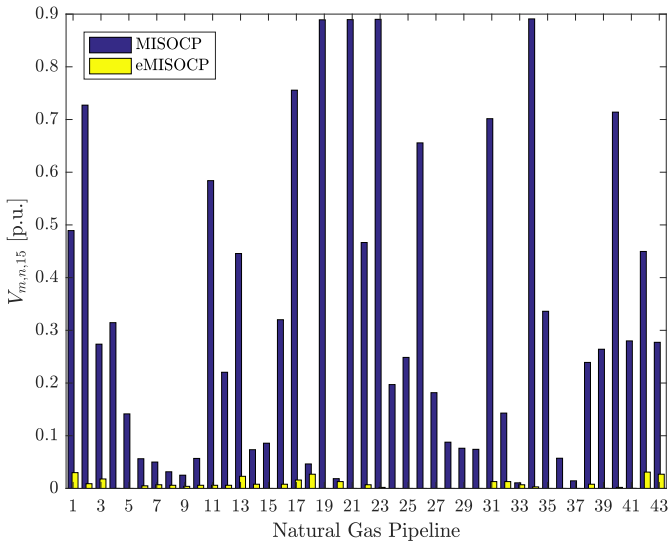

Fig. 8. Violations of constraints (12) for all natural gas pipelines in hour 15 in the case study in Section V.

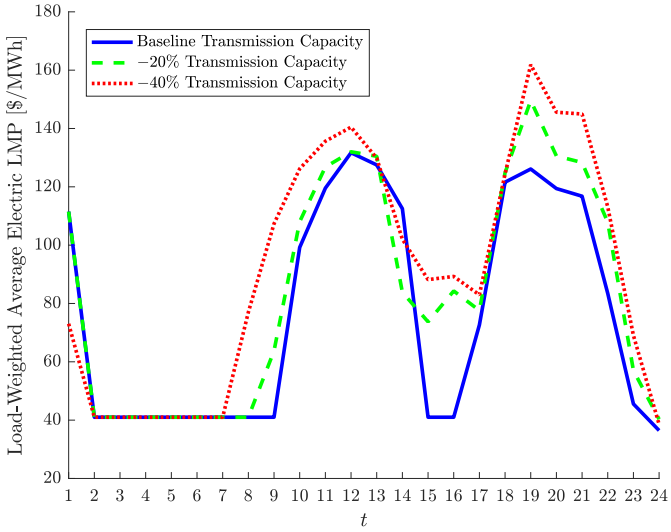

Fig. 9. Load-weighted average electric LMPs obtained from applying eMISOCP to the case study in Section V.

VI. CONCLUSION

This paper presents a unit commitment model that integrates non-convex nonlinear natural gas-flow equations that capture pipeline line-pack. We employ an enhanced convex relaxation to make the model tractable while obtaining high-quality solutions. The relaxation is obtained by using convex envelopes of bilinear terms in the natural gas-flow equations. This allows us to model 'both sides' of the equality. This can be contrasted with other convexification techniques, which only include one

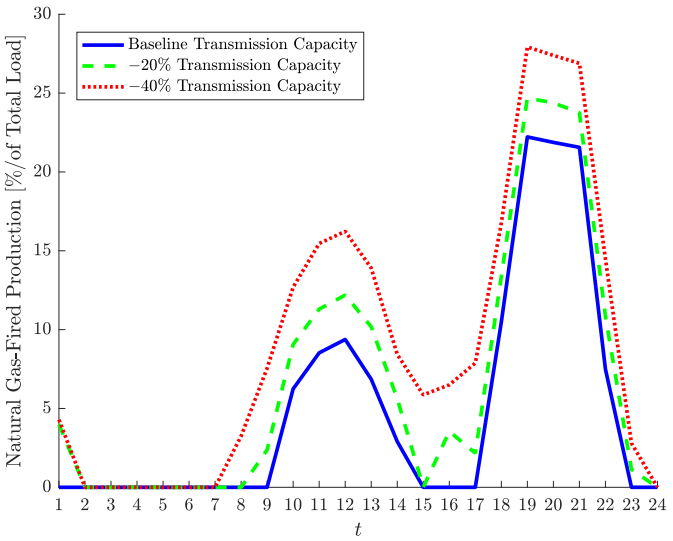

Fig. 10. Natural gas-fired electricity produced as a percentage of total electric load from applying eMISOCP to the case study in Section V.

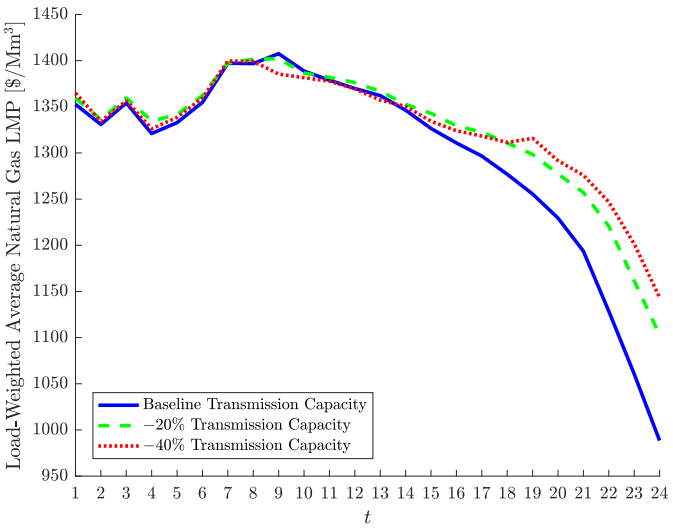

Fig. 11. Load-weighted average natural gas LMPs obtained from applying eMISOCP to the case study in Section V.

of the two inequalities that equivalently define the natural gas-flow equations. Electric and natural gas LMPs can be obtained by fixing the binary variables to their optimal values and employing a linearization of the non-linear flow equality. Test results demonstrate that the proposed eMISOCP yields higher-quality solutions compared to the MISOCP, especially as the convex envelopes are tightened using Algorithm 1.

We investigate the interdependencies between prices in the two systems. We find that congestion in one system can affect prices in the other. Moreover, this effect can be bidirectional. In the example in Section IV high natural gas demands force curtailment of natural gas loads, which significantly increases natural gas LMPs. This, in turn, makes natural gas-fired units more expensive, decreasing their use while at the same time increasing electric LMPs. These dynamics are reversed in the case study in Section V. In the case study, natural gas-fired units are relatively expensive and are only used to produce energy if absolutely necessary (*i.e.*, other lower-cost units are capacitated or transmission congestion requires the use of natural gas-fired units). Limited transmission capacity exactly forces such increased use of the natural gas-fired units. This increases both electric and natural gas LMPs (the latter effect owing to increased demand for natural gas due to electricity-production needs). Natural gas and electric power systems are currently operated independently of one another. Thus, our proposed model (and the existing literature to which it adds) does not have a present-day user. However, our and other works can be used to understand the importance of co-ordinating the operation of the two systems and the suboptimality (or potential reliability issues) that operating the systems independently of one another raise. Such analyses will be important formative steps in determining whether tighter co-optimization of the two systems should be pursued.

ACKNOWLEDGMENT

Thank you to the editors and four reviewers for helpful suggestions, comments, and conversations. The third author thanks A. Sorooshian for the same.

REFERENCES

[1] J. Yang, N. Zhang, C. Kang, and Q. Xia, "Effect of Natural Gas Flow Dynamics in Robust Generation Scheduling Under Wind Uncertainty," *IEEE Transactions on Power Systems*, vol. 33, pp. 2087–2097, March 2018.

[2] R. Chen, J. Wang, and H. Sun, "Clearing and Pricing for Coordinated Gas and Electricity Day-Ahead Markets Considering Wind Power Uncertainty," *IEEE Transactions on Power Systems*, vol. 33, pp. 2496–2508, May 2018.

[3] A. Quelhas, E. Gil, J. D. McCalley, and S. M. Ryan, "A Multiperiod Generalized Network Flow Model of the U.S. Integrated Energy System: Part I—Model Description," *IEEE Transactions on Power Systems*, vol. 22, pp. 829–836, May 2007.

[4] J. Wu, J. Yan, H. Jia, N. Hatziargyriou, N. Djilali, and H. Sun, "Integrated Energy Systems," *Applied Energy*, vol. 167, pp. 155–157, 1 April 2016.

[5] S. Chen, Z. Wei, G. Sun, K. W. Cheung, and Y. Sun, "Multi-Linear Probabilistic Energy Flow Analysis of Integrated Electrical and Natural-Gas Systems," *IEEE Transactions on Power Systems*, vol. 32, pp. 1970–1979, May 2017.

[6] P. J. Hibbard and T. Schatzki, "The Interdependence of Electricity and Natural Gas: Current Factors and Future Prospects," *The Electricity Journal*, vol. 25, pp. 6–17, May 2012.

[7] C. Liu, M. Shahidehpour, Y. Fu, and Z. Li, "Security-Constrained Unit Commitment With Natural Gas Transmission Constraints," *IEEE Transactions on Power Systems*, vol. 24, pp. 1523–1536, August 2009.

[8] C. Liu, M. Shahidehpour, and J. Wang, "Coordinated scheduling of electricity and natural gas infrastructures with a transient model for natural gas flow," *Chaos: An Interdisciplinary Journal of Nonlinear Science*, vol. 21, p. 025102, 6 2011.

[9] B. Zhao, A. J. Conejo, and R. Sioshansi, "Unit Commitment Under Gas-Supply Uncertainty and Gas-Price Variability," *IEEE Transactions on Power Systems*, vol. 32, pp. 2394–2405, May 2017.

[10] X. Zhang, M. Shahidehpour, A. Alabdulwahab, and A. Abusorrah, "Hourly Electricity Demand Response in the Stochastic Day-Ahead Scheduling of Coordinated Electricity and Natural Gas Networks," *IEEE Transactions on Power Systems*, vol. 31, pp. 592–601, January 2016.

[11] C. M. Correa-Posada, P. Sánchez-Martín, and S. Lumbreras, "Security-constrained model for integrated power and natural-gas system," *Journal of Modern Power Systems and Clean Energy*, vol. 5, pp. 326–336, May 2017.

[12] Y. He, M. Shahidehpour, Z. Li, C. Guo, and B. Zhu, "Robust Constrained Operation of Integrated Electricity-Natural Gas System Considering Distributed Natural Gas Storage," *IEEE Transactions on Sustainable Energy*, vol. 9, pp. 1061–1071, July 2018.

[13] A. Antenucci and G. Sansavini, "Gas-Constrained Secure Reserve Allocation With Large Renewable Penetration," *IEEE Transactions on Sustainable Energy*, vol. 9, pp. 685–694, April 2018.
[14] C. B. Sánchez, R. Bent, S. Backhaus, S. Blumsack, H. Hijazi, and P. van Hentenryck, "Convex Optimization for Joint Expansion Planning of Natural Gas and Power Systems," in *49th Hawaii International Conference on System Sciences*, Koloa, Hawaii, 5-8 January 2016, pp. 2536–2545.
[15] S. Chen, Z. Wei, G. Sun, D. Wang, and H. Zang, "Steady state and transient simulation for electricity-gas integrated energy systems by using convex optimisation," *IET Generation, Transmission & Distribution*, vol. 12, pp. 2199–2206, 15 May 2018.
[16] S. Chen, Z. Wei, G. Sun, D. Wang, Y. Zhang, and Z. Ma, "Stochastic look-ahead dispatch for coupled electricity and natural-gas networks," *Electric Power Systems Research*, vol. 164, pp. 159–166, November 2018.
[17] C. Wang, W. Wei, J. Wang, L. Wu, and Y. Liang, "Equilibrium of Interdependent Gas and Electricity Markets with Marginal Price Based Bilateral Energy Trading," *IEEE Transactions on Power Systems*, vol. 33, pp. 4854–4867, September 2018.
[18] A. Zlotnik, L. Roald, S. Backhaus, M. Chertkov, and G. Andersson, "Control Policies for Operational Coordination of Electric Power and Natural Gas Transmission Systems," in *2016 American Control Conference*. Boston, Massachusetts: Institute of Electrical and Electronics Engineers, 6-8 July 2016, pp. 7478–7483.
[19] C. M. Correa-Posada and P. Sánchez-Martín, "Integrated Power and Natural Gas Model for Energy Adequacy in Short-Term Operation," *IEEE Transactions on Power Systems*, vol. 30, pp. 3347–3355, November 2015.
[20] K. Sundar and A. Zlotnik, "State and Parameter Estimation for Natural Gas Pipeline Networks Using Transient State Data," *IEEE Transactions on Control Systems Technology*, 2019, in press.
[21] O. Massol and A. Banal-Estañol, "Market Power and Spatial Arbitrage between Interconnected Gas Hubs," *The Energy Journal*, vol. 39, pp. 67–95, 2018.
[22] A. Ben-Tal and A. Nemirovski, *Lectures on Modern Convex Optimization: Analysis, Algorithms, and Engineering Applications*, ser. MOS-SIAM Series on Optimization. Philadelphia, Pennsylvania: Society for Industrial and Applied Mathematics, 2001.
[23] G. P. McCormick, "Computability of global solutions to factorable nonconvex programs: Part I—Convex underestimating problems," *Mathematical Programming*, vol. 10, pp. 147–175, December 1976.
[24] C. Coffrin, H. L. Hijazi, and P. V. Hentenryck, "The QC Relaxation: A Theoretical and Computational Study on Optimal Power Flow," *IEEE Transactions on Power Systems*, vol. 31, pp. 3008–3018, July 2016.
[25] M. F. Anjos and J. B. Lasserre, Eds., *Handbook on Semidefinite, Conic and Polynomial Optimization*, 1st ed., ser. International Series in Operations Research & Management Science. New York, New York: Springer US, 2012, vol. 166.
[26] S. Wu, R. Z. Ríos-Mercado, E. A. Boyd, and L. R. Scott, "Model relaxations for the fuel cost minimization of steady-state gas pipeline networks," *Mathematical and Computer Modelling*, vol. 31, pp. 197–220, January-February 2000.

Sheng Chen (S'16) received his B.S. degree from the College of Energy and Electrical Engineering, Hohai University, Nanjing, China, in 2014, where he is currently pursuing the Ph.D. degree. From January 2018 to January 2019 he was a visiting scholar at The Ohio State University, Columbus, OH.

His research interests include integrated energy systems, operations research, and electricity markets.

Antonio J. Conejo (F'04) received the M.S. degree from the Massachusetts Institute of Technology, Cambridge, MA, in 1987, and the Ph.D. degree from the Royal Institute of Technology, Stockholm, Sweden, in 1990.

He is currently a professor in the Department of Integrated Systems Engineering and the Department of Electrical and Computer Engineering, The Ohio State University, Columbus, OH. His research interests include control, operations, planning, economics and regulation of electric energy systems, as well as statistics and optimization theory and its applications.

Ramteen Sioshansi (M'11–SM'12) holds the B.A. degree in economics and applied mathematics and the M.S. and Ph.D. degrees in industrial engineering and operations research from the University of California, Berkeley, and an M.Sc. in econometrics and mathematical economics from The London School of Economics and Political Science.

He is a professor in the Department of Integrated Systems Engineering at The Ohio State University, Columbus, OH. His research focuses on renewable and sustainable energy system analysis and the design of restructured competitive electricity markets.

Zhinong Wei received the B.S. degree from Hefei University of Technology, Hefei, China, in 1984, the M.S. degree from Southeast University, Nanjing, China, in 1987, and the Ph.D. degree from Hohai University, Nanjing, China, in 2004.

He is now a professor of electrical engineering with the College of Energy and Electrical Engineering, Hohai University, Nanjing, China. His research interests include integrated energy systems, power system state estimation, smart distribution systems, and integration of distributed generation into electric power systems.